

Top vs. Bottom Charging of the Dielectric in RF MEMS Capacitive Switches

Zhen Peng¹, Xiaobin Yuan¹, James C. M. Hwang¹, David Forehand² and Charles L. Goldsmith²

¹Lehigh University, Bethlehem, PA 18015, USA

²MEMtronics Corp., Plano, TX 75075, USA

Tel: +1-610-758-5104, Fax: +1-610-758-4244, E-mail: jh00@lehigh.edu

Abstract — Using a movable top electrode, for the first time, top vs. bottom charging of the dielectric in metal/insulator/metal capacitors is delineated. For the Al/SiO₂/Cr structure used in RF MEMS capacitive switches, charge injection from Al into the top of SiO₂ was found to have a higher threshold voltage, faster charging time, and slower discharging time than charge injection from Cr into the bottom of SiO₂. The higher threshold is attributed to non-ideal contact geometry and chemistry. The faster charging time is attributed to the exponential voltage dependence. The slower discharging time is attributed to diffusion across SiO₂. Since top charging is more critical to switch performance and reliability than bottom charging, understanding the trade off of top vs. bottom charging can help minimize their undesirable effects.

Index Terms — Charging, dielectric, RF MEMS, switch, trap.

I. INTRODUCTION

MEMS switches can potentially replace GaAs transistors and diodes in switching RF signals [1], [2]. However, in many cases, the lifetime of RF MEMS capacitive switches is limited by dielectric charging [3]-[15]. During switch operation, the control voltage across the dielectric causes charge to be injected into the dielectric and become trapped. With repeated operation, charge gradually builds up in the dielectric, which modifies the electrostatic force on the movable electrode and results in actuation-voltage shift and stiction. For RF MEMS capacitive switches based on the Al/SiO₂/Cr structure, we have characterized [10] charge injection from the bottom Cr electrode into the SiO₂ under moderate control voltages. We now report operation of similar switches under higher control voltages, which causes charge injection from the top Al electrode into the SiO₂, in addition to charge injection from the bottom Cr electrode similar to that reported in [10].

II. EXPERIMENTAL

Fig. 1 illustrates the cross section of an RF MEMS capacitive switch fabricated on a glass substrate. The dielectric is sputtered SiO₂ with a thickness of 0.25 μm and a dielectric constant of 4.0. The top electrode is a 0.3-μm-thick Al membrane that is grounded. The bottom Cr/Au electrode serves as the center conductor of a 50 Ω coplanar waveguide for the RF signal. Without any control voltage applied, the

membrane is normally suspended in air approximately 2.5 μm above the dielectric. A control voltage is applied to the bottom electrode, which pulls the membrane into contact with the SiO₂ thus forming a 120 μm x 80 μm capacitor to shunt the RF signal to ground. To characterize charging effects, the switch was stressed with different control voltages and polarities at room temperature and less than 1% relative humidity. During each stress period, the shift in actuation voltage was periodically sampled by applying a triangular voltage pulse while monitoring the RF signal output [7].

III. CHARGING UNDER POSITIVE CONTROL VOLTAGES

Fig. 2 shows measured actuation-voltage shifts during and after stresses at 30, 40 and 50 V for 300 s. The actuation voltage for a pristine switch is 26 V. When the switch is stressed at 30 V, the actuation voltage decreases gradually by approximately 5 mV/s. This indicates that positive charge is injected from the bottom electrode into the dielectric, which enhances the electrostatic force on the top electrode when a positive control voltage is applied to the bottom electrode. After the 30 V stress is removed, the bottom-injected charge gradually discharges and the actuation voltage recovers to its pristine value of 26 V within approximately 1000 s. When the switch is stressed at 40 V, the actuation voltage shifts and recovers in a similar manner to that at 30 V. However, the

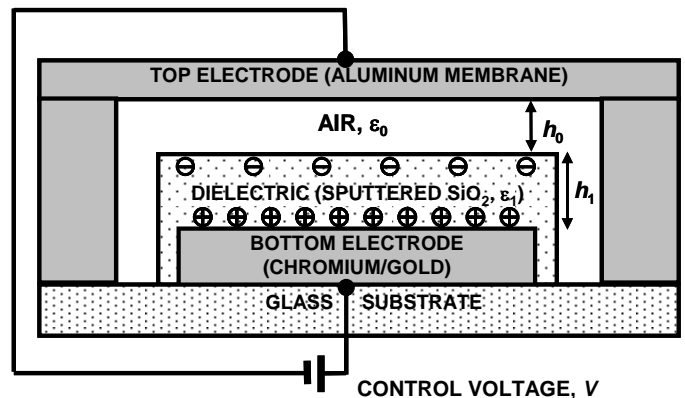


Fig. 1. Schematic cross section of an RF MEMS capacitive switch. Charge injection into the top and bottom of the dielectric is indicated for the case of a positive control voltage.

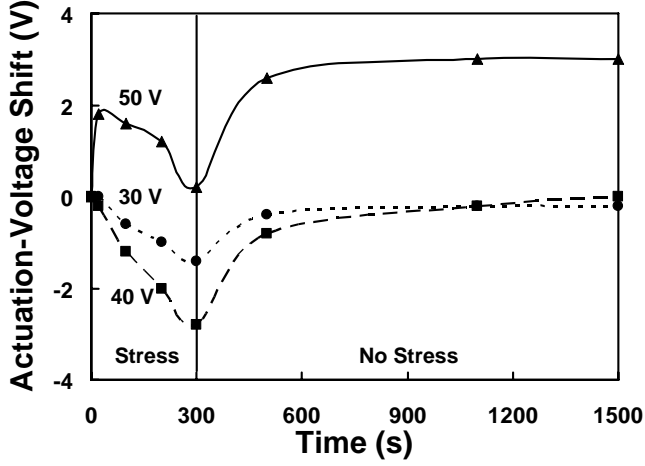


Fig. 2. Shifts in actuation voltage magnitude during and after (●) 30, (■) 40, and (▲) 50 V stresses, respectively.

actuation-voltage shift is larger than that at 30 V, which is consistent with the previously reported exponential dependence of charging on voltage [10]. Despite being larger, the actuation-voltage shift at 40 V also recovers within approximately 1000 s, which is consistent with the previously reported independence of discharging times on voltage [10].

The above-described stress results under 30 and 40 V are consistent with the bottom-charging mechanism reported in [10]. By contrast, when the switch is stressed at 50 V, the results are qualitatively different so that a top-charging mechanism must be invoked in addition to the bottom-charging mechanism. Fig. 2 shows that, under 50 V, the actuation voltage quickly increases before gradually decreases. At the end of the 300 s stress period, the net actuation-voltage shift is almost nil. After the 50 V stress is removed, the actuation voltage gradually increases by approximately 3 V in ~1000 s. This suggests that, under the 50 V stress, in addition to positive charge being injected from the bottom electrode into the dielectric, negative charge is also injected from the top electrode into the dielectric. Furthermore, top charging is much faster than bottom charging, while discharging of top-injected charge is much slower than discharging of bottom-injected charge. Thus, when the 50 V is applied to the bottom electrode, negative charge is quickly injected from the top electrode into the dielectric. Within a few seconds, top charging saturates or otherwise slows down to allow positive charge from the bottom to catch up and to gradually compensate for the effect that is caused by the negative charge injected from the top. After the 50 V stress is removed, the bottom-injected charge discharges in ~1000 s similar to the 30 and 40 V cases. However, with the top electrode up in the air, the top-injected charge must diffuse across the thickness of the dielectric in order to be discharged. Fig. 3 shows that, after the 50 V stress,

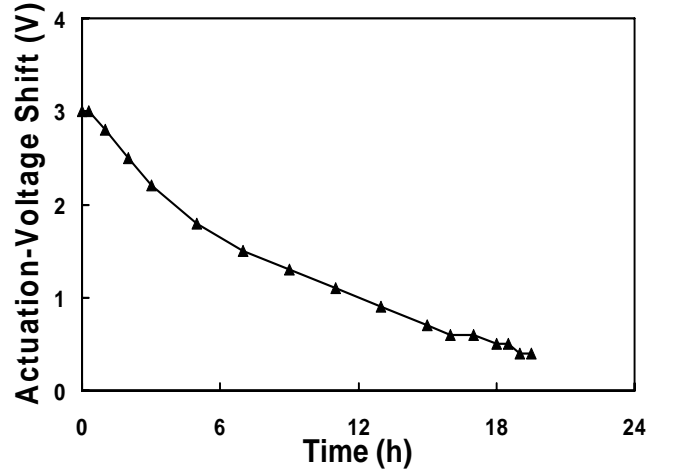


Fig. 3. Recovery of actuation-voltage shift after 50 V stress for 300 s.

it took many hours for the actuation voltage to recover to its pristine value.

The top- and bottom-injected charges, Q_T and Q_B , can be modeled as [10]:

$$Q_T = Q_{T0} [1 - \exp(-t_{ON} / \tau_{CT})] \exp(-t_{OFF} / \tau_{DT}) \quad (1)$$

$$Q_B = Q_{B0} [1 - \exp(-t_{ON} / \tau_{CB})] \exp(-t_{OFF} / \tau_{DB}) \quad (2)$$

where T and B denote top and bottom, respectively. Q_0 is the steady-state charge. τ_C and τ_D are charging and discharging time constants, respectively. t_{ON} and t_{OFF} are on and off times of the switch, respectively. Previously, τ_{CB} and τ_{DB} were found [10] to be of the order of 10 s. We now observe that $\tau_{CT} \ll \tau_{CB}$ and $\tau_{DT} \gg \tau_{DB}$. The actuation-voltage shift ΔV due to the combined effects of top charging and bottom charging is:

$$\Delta V = \frac{h_T Q_T - h_B Q_B}{\epsilon_0 \epsilon_1} \quad (3)$$

where ϵ_0 is the permittivity of vacuum; ϵ_1 is the relative dielectric constant. h_T and h_B are distances between the bottom electrode and top- and bottom-injected charges, respectively, assuming that the effect of the injected charge can be approximated by a sheet charge concentrated at the distance h . Notice that the effects of Q_T and Q_B are weighted by h_T and h_B , respectively. While there is no way to directly measure the distribution of the injected charge in the dielectric, a reasonable assumption is that $h_T \gg h_B$. Therefore, the fact that bottom charging can compensate for top charging suggests that $Q_T \ll Q_B$. In addition, based on a rough estimate of $\tau \sim h^2/D$ (D is diffusivity), it is not surprising that $\tau_{DT} \gg \tau_{DB}$. Presently we cannot explain why $\tau_{CT} \ll \tau_{CB}$ or why $Q_T \ll Q_B$. This suggests that the top-charging mechanism is rather different from the bottom-charging mechanism and more detailed investigation is necessary in the future.

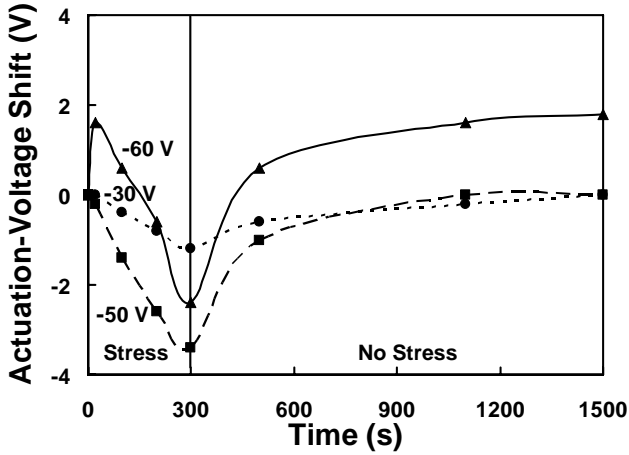


Fig. 4. Shifts in actuation voltage magnitude during and after (●) -30, (■) -50, and (▲) -60 V stresses, respectively.

IV. CHARGING UNDER NEGATIVE CONTROL VOLTAGES

Previously, we reported [10] that bottom-charging behaviors were similar under both positive and negative stresses. We now observe that top-charging behaviors are also similar under both positive and negative stresses, except the threshold voltage for top charging is a little higher under negative stress than under positive stress. Fig. 4 shows measured actuation-voltage shifts during and after stresses at -30, -50, and -60 V, respectively. To facilitate comparison with the positive-stress cases of Fig. 2, shifts in the absolute magnitude of actuation voltages are plotted. For example, the actuation voltage for the pristine switch is -26 V and a -1 V actuation-voltage shift means that the actuation voltage is shifted to -25 V. Between -30 and -50 V, bottom charging dominates. Top charging occurs only when the stress is increased to -60 V. The difference in top-charging thresholds may be explained by the energy band diagram of the Al/SiO₂/Cr structure. As shown in Fig. 5, the emission barriers from Al into SiO₂ are approximately 3.4 and 5.6 eV for electrons and holes, respectively. This explains why it is easier to inject electrons from Al into SiO₂ under positive voltages than to inject holes from Al into SiO₂ under negative voltages. However, the band diagram cannot be used to explain why 1) top-charging threshold is higher than bottom-charging threshold, 2) top-charging density is lower than bottom-charging density, or 3) bottom charging thresholds are similar under both positive and negative stresses. Therefore, we postulate that direct tunneling from the electrodes to the defect states in the dielectric plays a key role here. For tunneling, surface contamination of the dielectric can increase the top-charging threshold while the less than 100% contact area can decrease the top-charging density. These subjects are currently under investigation.

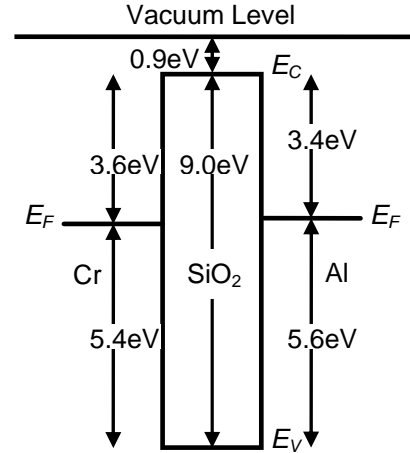


Fig. 5. Energy band diagram of the Al/SiO₂/Cr capacitor structure

V. CONCLUSION

In summary, the present Al/SiO₂/Cr structure has a higher threshold for top charging than for bottom charging. When the control voltage exceeds the top-charging threshold, charging occurs at both the top and bottom of SiO₂. Top charging is faster than bottom charging, but the former saturates at a lower density than the latter. Because the top-injected charge is closer to the movable top electrode and is slower to discharge, it has a greater impact on switch operation. For the present Al/SiO₂/Cr structure, the top-charging threshold of ~45 V is significantly higher than the actuation voltage of 26 V, so that a control voltage of ~30 V can be used to accommodate device-to-device variation and small actuation-voltage shift due to bottom charging, without causing top charging. For other cases where top charging is unavoidable, especially under complex control-voltage waveforms, the previously reported bottom-charging model [10] needs to be extended to include both top and bottom charging.

Charging in metal/insulator/metal capacitor structures has been studied extensively by the semiconductor industry and the combined effects of top and bottom charging have been reported [16]. By using a movable top electrode, for the first time, top charging can be delineated from bottom charging. This will have a significant impact on not only MEMS devices, but also many other electronic devices.

ACKNOWLEDGEMENT

This work was partially supported by the US Air Force Research Laboratory under Contract No. F33615-03-C-7003. The contract was funded by the US Defense Advanced Research Projects Agency under the Harsh Environment, Robust Micromechanical Technology Program.

REFERENCES

- [1] C. Goldsmith, Z. Yao, S. Eshelman, and D. Denniston, "Performance of low-loss RF MEMS capacitive switches," *IEEE Microwave Guided Wave Lett.*, vol. 8, no. 8, pp. 269-271, Aug. 1998.
- [2] D. Peroulis, S. Pacheco, and L. P. B. Katehi, "MEMS devices for high isolation switching and tunable filtering," *IEEE MTT-S Int. Microwave Symp. Dig.*, pp. 1217-1220, June 2000.
- [3] C. Goldsmith, J. Ehmke, A. Malczewski, B. Pillans, S. Eshelman, Z. Yao, J. Brank, and M. Eberly, "Lifetime characterization of capacitive RF MEMS switches," *IEEE MTT-S Int. Microwave Symp. Dig.*, pp. 227-230, June 2001.
- [4] J. R. Reid, and R. T. Webster, "Measurements of charging in capacitive Microelectromechanical switches," *Electron. Lett.*, vol. 38, no. 24, pp. 1544-1545, Nov. 2002.
- [5] W. M. van Spengen, R. Puers, R. Mertens, and I. De Wolf, "Experimental characterization of stiction due to charging in RF MEMS," *IEEE Int. Electron Devices Meet. Dig.*, pp. 901-904, Dec. 2002.
- [6] W. M. van Spengen, R. Puers, R. Mertens, and I. De Wolf, "A comprehensive model to predict the charging and reliability of capacitive RF MEMS switches," *J. Micromech. Microeng.*, vol. 14, pp. 514-521, Jan. 2004.
- [7] X. Yuan, S. V. Cherepko, J. C. M. Hwang, C. L. Goldsmith, C. Nordquist, and C. Dyck, "Initial observation and analysis of dielectric-charging effects on RF MEMS capacitive switches," *IEEE MTT-S Int. Microwave Symp. Dig.*, pp. 1943-1946, June 2004.
- [8] D. Dubuc, W. M. van Spengen, S. Melle, I. De Wolf, R. Mertens, P. Pons, K. Grenier, and R. Plana, "Methodology to assess the reliability behavior of RF-MEMS," *GAAS 12th Symp. Dig.*, pp. 459-462, Oct. 2004.
- [9] X. Rottenberg, B. Nauwelaers, W. Raedt, and H.A.C. Tilmans, "Distributed dielectric charging and its impact on RF-MEMS device," *GAAS 12th Symp. Dig.*, pp. 475-478, Oct. 2004.
- [10] X. Yuan, J. C. M. Hwang, D. Forehand, and C. L. Goldsmith, "Modeling and characterization of dielectric-charging effects in RF MEMS capacitive switches," *IEEE MTT-S Int. Microwave Symp. Dig.*, pp. 753-756, June 2005.
- [11] S. Melle, D. De Conto, L. Mazonq, D. Dubuc, K. Grenier, L. Bary, O. Vendier, J.L. Cazaux, and R. Plana, "Modeling of the dielectric charging kinetic for capacitives RF-MEMS," *IEEE MTT-S Int. Microwave Symp. Dig.*, pp. 757-760, June 2005.
- [12] G. J. Papaioannou, M. Exarchos, V. Theonas, G. Wang, and J. Papapolymerou, "On the dielectric polarization effects in capacitive RF-MEMS switches," *IEEE MTT-S Int. Microwave Symp. Dig.*, pp. 761-764, June 2005.
- [13] G. J. Papaioannou, M. Exarchos, V. Theonas, G. Wang, and J. Papapolymerou, "Temperature study of the dielectric polarization effects of capacitive RF-MEMS switches," *IEEE Trans. Microwave Theory Techniques*, vol. 53, pp. 3467-3473, Nov. 2005.
- [14] R. W. Herfst, H. G. A. Huizing, P. G. Steeneken, and J. Schnitz, "Characterization of dielectric charging in RF MEMS capacitive switches," *IEEE Int. Conf. on Microelectronic Test Structures*, pp. 133-136, Mar. 2006.
- [15] J. F. Kcko, J. C. Petrosky, J. R. Reid and K. Yung, "Non-charge related mechanism affecting capacitive MEMS switch lifetime," *IEEE Microwave Wireless Components Lett.*, vol. 16, no. 3, pp. 140-142, Mar. 2006.
- [16] D. L. Smith, A. S. Alimonda, C.-C. Chen, and H. C. Tuan, "Reduction of charge injection into PECVD SiN_xH_y by control of deposition chemistry," *J. Electronic Materials*, vol. 19, no. 1, pp. 19-27, 1990.